Foscan and Foslip based photodynamic therapy in osteosarcoma in vitro and in intratibial mouse models

Meier, Daniela ; Botter, Sander M ; Campanile, Carmen ; Robl, Bernhard ; Gräfe, Susanna ; Pellegrini, Giovanni ; Born, Walter ; Fuchs, Bruno

Abstract: Current osteosarcoma therapies cause severe treatment-related side effects and chemoresistance, and have low success rates. Consequently, alternative treatment options are urgently needed. Photodynamic therapy (PDT) is a minimally invasive, local therapy with proven clinical efficacy for a variety of tumor types. PDT is cytotoxic, provokes anti-vascular effects and stimulates tumor cell targeting mechanisms of the immune system and, consequently, has potential as a novel therapy for osteosarcoma patients. This study investigated the uptake and the dark- and phototoxicity and cytotoxic mechanisms of the photosensitizer (PS) 5,10,15,20-tetrakis(meta-hydroxyphenyl) chlorine (mTHPC, Foscan) and a liposomal mTHPC formulation (Foslip) in the human 143B and a mouse K7M2-derived osteosaroma cell line (K7M2L2) in vitro. Secondly the tumor- and metastasis-suppressive efficacies of mTHPC formulations based PDT and associated mechanisms in intratibial, metastasizing osteosarcoma mouse models (143B/SCID and syngeneic K7M2L2/BALB/c) were studied. The uptake of Foscan and Foslip in vitro was time- and dose-dependent and resulted in mTHPC and light dose-dependent phototoxicity associated with apoptosis. In vivo, the uptake of both i.v. administered mTHPC formulations was higher in tumor than in healthy control tissue. PDT caused significant (Foscan $P<0.05$, Foslip $P<0.001$) tumor growth inhibition in both models. A significant (Foscan $P<0.001$, Foslip $P<0.001$) immunsystem-dependent suppression of lung metastasis was only observed in the K7M2L2/BALB/c model and was associated with a marked infiltration of T-lymphocytes at the primary tumor site.

DOI: https://doi.org/10.1002/ijc.30572

Foscan and Foslip based photodynamic therapy in osteosarcoma *in vitro* and in intratibial mouse models

Daniela Meier[1], Sander M. Botter[1], Carmen Campanile[1], Bernhard Robl[1], Susanna Gräfe[3], Giovanni Pellegrini[2], Walter Born[1], Bruno Fuchs[1].

[1] Laboratory for Orthopedic Research, Department of Orthopedics, Balgrist University Hospital, Zurich, Switzerland

[2] Laboratory for Animal Model Pathology, Institute of Veterinary Pathology, University of Zurich, Zurich, Switzerland

[3] Biolitec Research GmbH, Otto-Schott-Straße 15, Jena, Germany

*Corresponding author e-mail: bfuchs@research.balgrist.ch (Bruno Fuchs)

Short title: Foscan and Foslip based photodynamic therapy in osteosarcoma.

Novelty and impact: Osteosarcoma is a devastating disease associated with impaired survival rates and treatment induced side effects, due to high tumor heterogeneity, chemoresistance and drug toxicity. We suggest photodynamic therapy using Foscan and its liposomal formulation Foslip as a novel approach for the treatment of metastasizing osteosarcoma. The present study demonstrates the inhibition of tumor growth and immune system-dependent suppression of metastatic spread by PDT with Foscan and Foslip in two different clinical relevant osteosarcoma mouse models.

Key words: osteosarcoma, photodynamic therapy, Foslip, Foscan, metastasis

Abbreviations: 5-ysr: five-year survival rate; ANOVA: analysis of variance; CC: cleaved caspase; CD31: cluster of differentiation 31; HE: hematoxylin & eosin; IC50: half-maximal inhibitory concentration; i.p.: intraperitoneally; i.v.: intravenous; mTHPC: 5,10,15,20-

tetrakis(meta-hydroxyphenyl)chlorine; PDT: photodynamic therapy; PS: photosensitizer; RFU: relative fluorescence unit; ROI: region of interest; WST-1: water-soluble tetrazolium; X-Gal: 5-bromo-4-chloro-3-indolyl-beta-D-galacto-pyranoside

Article category: Research Article, Cancer Therapy and Prevention

Conflict of interest: The Authors declare that there is no conflict of interest

Abstract

Current osteosarcoma therapies cause severe treatment-related side effects and chemoresistance, and have low success rates. Consequently, alternative treatment options are urgently needed. Photodynamic therapy (PDT) is a minimally invasive, local therapy with proven clinical efficacy for a variety of tumor types. PDT is cytotoxic, provokes anti-vascular effects and stimulates tumor cell targeting mechanisms of the immune system and, consequently, has potential as a novel therapy for osteosarcoma patients. This study investigated the uptake and the dark- and phototoxicity and cytotoxic mechanisms of the photosensitizer (PS) 5,10,15,20-tetrakis(meta-hydroxyphenyl) chlorine (mTHPC, Foscan) and a liposomal mTHPC formulation (Foslip) in the human 143B and a mouse K7M2-derived osteosaroma cell line (K7M2L2) *in vitro*. Secondly the tumor- and metastasis-suppressive efficacies of mTHPC formulations based PDT and associated mechanisms in intratibial, metastasizing osteosarcoma mouse models (143B/SCID and syngeneic K7M2L2/BALB/c) were studied. The uptake of Foscan and Foslip *in vitro* was time- and dose-dependent and resulted in mTHPC and light dose-dependent phototoxicity associated with apoptosis. *In vivo,* the uptake of both i.v. administered mTHPC formulations was higher in tumor than in healthy control tissue. PDT caused significant (Foscan $P<0.05$, Foslip $P<0.001$) tumor growth inhibition in both models. A significant (Foscan $P<0.001$, Foslip $P<0.001$) immunsystem-dependent suppression of lung metastasis was only observed in the K7M2L2/BALB/c model and was associated with a marked infiltration of T-lymphocytes at the primary tumor site.

In conclusion, mTHPC-based PDT is effective in clinically relevant experimental osteosarcoma and suppresses lung metastasis in immunocompetent mice with beneficial effects of the liposomal mTHPC formulation Foslip.

Introduction

Osteosarcoma is the most common primary high-grade bone neoplasm and one of the deadliest cancer types in children and adolescents[1, 2]. Since the introduction of new treatment protocols in the 70ies, including neoadjuvant and adjuvant chemotherapy, the 5-year survival rate (5-ysr) of patients with localized disease increased significantly to approximately 60% but plateaued ever since[3, 4]. However, patients with metastatic disease, with lesions most frequently developing in the lungs and other bones, continue to have a poor 5-ysr of approximately 30%[5]. Unfortunately, multi-drug therapy, using high-dose methotrexate, cisplatin, and doxorubicin, is associated with a variety of severe side effects ranging from gastrointestinal problems, neutropenia, cardiac toxicity, neurological dysfunction, second malignant neoplasms to even death[6, 7]. Although multi-agent chemotherapy increased the survival of patients, it plateaued over the last three decades, most probably owing to the high tumor heterogeneity of osteosarcoma and to chemoresistance[8, 9]. The lack of novel, more effective therapeutic strategies for metastasizing osteosarcoma has become an increasing problem.

During the last four decades, photodynamic therapy (PDT) evolved into a novel attractive treatment option for a variety of cancer types[10]. PDT is a multi-step process making use of three components; photosensitizer (PS), light and oxygen[11]. In a first step of the therapy, PS is injected into the blood stream and is taken up by tumor and also by healthy cells. Next, tumor-selective PDT is achieved by local illumination of the tumor site with light, which activates the light-sensitive PS to a higher energy state and results in the direct or indirect transfer of excess energy to neighboring oxygen molecules or tissue molecules, producing cell-toxic reactive oxygen. Finally, in addition to eliciting direct cytotoxicity, PDT provokes a variety of additional beneficial anti-tumor effects such as an acute inflammatory response, anti-

vascular effects and an activation of the immune system[11]. PDT has commonly been employed for the treatment of solid tumors at superficial anatomical locations, however, its application in other tumors at more inaccessible sites has become an aim of clinical investigations[12, 13]. Additionally to the advantage of PDT as a local application, also a systemic immune response against tumors have been reported[14-16], therefore PDT is potentially not only effective against local tumor growth but also against distant metastases.

PDT is associated with good functional and aesthetic outcomes and clinical studies reported it as a good treatment option for patients unsuitable for other treatments in head and neck cancers[17, 18], but studies investigating potential therapeutic applications in osteosarcoma are scarce. *In vitro* investigations demonstrated strong cytotoxic effects of PDT in different osteosarcoma cells lines[19-22]. Preclinical studies in osteosarcoma mouse models showed an inhibition of local tumor growth[23, 24], but these studies were either performed in subcutaneous osteosarcoma mouse models, which do not reproduce the clinical situation, or in immune suppressed mice, where the impact on distant metastases cannot be evaluated. Nevertheless, a preclinical study by Burch et al., who applied PDT in dogs that spontaneously developed osteosarcoma, demonstrated substantial tumor necrosis, indicating the potential of PDT for effective treatment of osteosarcoma, but long-term effects or treatment impact on metastases were not reported[25].

One of the most powerful and commonly used PS is 5,10,15,20-tetrakis(meta-hydroxyphenyl)chlorine (mTHPC), traded under the name Foscan®. Although mTHPC is a potent PS, its high hydrophobicity restricts the routes of administration. Encapsulation of mTHPC into liposomal structures, however, achieved with the formulation Foslip used in the present study, makes it water soluble, which potentially increases PDT efficacy[26-28].

In this study, we investigated the uptake and the dark- and phototoxicity of Foscan and Foslip in the human 143B and in a derivative (K7M2L2) of the mouse K7M2 osteosarcoma cell line. In addition, we studied the efficacies of Foscan- and Foslip-based PDT in a 143B cell line-dependent intratibial xenograft osteosarcoma model in SCID mice and in an intratibial K7M2L2 cell line-derived model in syngeneic, immune competent BALB/c mice. Tumors in both models metastasize to the lung. Thus, these models allowed us to compare the tumor- and metastasis-suppressive potential of Foscan- and Foslip-based PDT in the absence and in the presence of a functional immune system. The results demonstrated promising tumor and immune system-dependent metastasis suppressive effects and anti-vascular activity of the here applied PDT in a clinically relevant experimental osteosarcoma model.

Materials and Methods

Photosensitizer and OS cell lines

Foscan and Foslip were kindly provided by Biolitec research GmbH (Jena, Germany). Foscan was reconstituted and diluted in ethanol (40% w/w) and propylene glycol (60% w/w). Foslip, a liposomal formulation of mTHPC, is a 9:1 mixture of dipalmitoylphosphatidylcholine (DPPC) and dipalmitoylphosphatidylglycerol (DPPG; >99% purity). Foslip (freeze-dried product) was reconstituted with water to 1.5 mg mTHPC/ml and further diluted in 5% glucose.

Human 143B osteosarcoma cells were purchased from ECACC (Salisbury, UK) and murine K7M2 osteosarcoma cells (CRL-2836) were kindly provided by Dr. Chand Khanna (Center for Cancer Research National Institute, Bethesda, USA). Cells were cultured in DMEM (4.5 g/l glucose)/HamF12 (1:1) medium (Invitrogen, Carlsbad, CA), supplemented with 10% heat-inactivated FCS (GIBCO, Basel, Switzerland), at 37°C in a humidified atmosphere of 5% CO_2 air.

Both cell lines were transduced with a *lacZ* reporter gene[29]. 3 x 10^5 of K7M2/*lacZ* cells were intratibially (i.t.) injected into female, 8 week old BALB/c mice as described[30]. The K7M2L2/*lacZ* cell line was obtained after two rounds of *in vivo* selection of metastatic *lacZ* expressing cells within the lung according to Fidler's method[31].

Uptake of mTHPC *in vitro*

143B/*lacZ* and K7M2L2/*lacZ* (referred to as 143B and K7M2L2) cells were seeded in six well plates (2000 cells/well for dose dependent uptake and 800 cells/well for time-dependent uptake) and allowed to adhere overnight. In time-course experiments, cells were incubated under tissue culture conditions with Foscan or Foslip equivalent to 2.5 µg/ml mTHPC for 0 - 48 h. For dose-dependent uptake, the cells were incubated for 5 h in the dark in tissue culture medium containing PS formulations equivalent to 0 - 10µg/ml mTHPC. Subsequently, the cells were washed two times with 100 µl PBS before the fluorescence of the cells in 100 µl PBS was measured at 652 nm with excitation at 417 nm in a Spectramax Gemini XS plate reader (Molecular Devices, Sunnyvale, CA). Results were obtained as relative fluorescence unit (RFU).

Subcellular localization of mTHPC (Foscan and Foslip) was visualized by confocal laser scanning microscopy as previously described[19]. Cells were stained with Hoechst (Life Technologies, Carlsbad, USA).

Cytotoxicity assay

143B and K7M2L2 cells (2500 cells / well) were incubated under tissue culture conditions for 5 h at different concentrations of Foslip or Foscan (0 - 200 µg/ml mTHPC) and left untreated in the dark or illuminated with 652 nm laser light at an energy dose of 1 J/cm^2 or 5 J/cm^2 (21.88 mW/cm^2) as described previously[19]. 24 hours later, the cell viability was measured with the water-

soluble tetrazolium (WST-1) assay (Roche, Basel, Switzerland) according to the manufacturer's protocol.

Western Blot analysis of apoptosis

10^6 143B or K7M2L2 cells were seeded in 6 cm cell culture dishes. After overnight adherence, cells were incubated under tissue culture conditions for 5 h with Foscan or Foslip (0.6 µg/ml mTHPC) and pre-incubated for 1 h with or without the pan-caspase inhibitor Z-VAD-FMK (100 µM) or its solvent control (1% DMSO) (BD Pharmingen AG, Allschwil, Switzerland). Cells were illuminated and protein extracts were analyzed for PARP and cleaved PARP (1:1000, Cell Signaling Technology) and GAPDH (protein loading control) (1:3000, Santa Cruz Biotechnologies, Texas, USA) as previously described[19].

Intratibial human xenograft and syngeneic osteosarcoma mouse models

All studies were conducted with the approval of the Veterinary Office Kanton Zurich, Switzerland (animal application license 167/2012) and in accordance with the guidelines of the Swiss Federal Veterinary Office. Eight-week-old female SCID and BALB/c mice were obtained from Charles River Laboratories. 10^5 143B/*lacZ* cells in 10 µl PBS/0.05% EDTA were injected i.t. into SCID mice (143B/SCID) (human xenograft mouse model) and 10^5 K7M2L2/*lacZ* cells in 10 µl PBS/0.05% EDTA i.t. into BALB/c mice (K7M2L2/BALB/c) (syngeneic mouse model) as previously described[30].

***In vivo* uptake of Foscan and Foslip by intratibial tumors**

Upon formation of a tumor (>50 mm^3), Foscan or Foslip at doses equivalent to 1.5 mg/kg mTHPC were administered to the mice (143B/SCID n=10, K7M2L2/BALB/c n=14) with a slow (4-6 min) intravenous (i.v.) injection in the tail vein. The mice were then kept in a darkened environment for

the rest of the experiment. The area of the leg where the tumor was localized was shaved and the mTHPC uptake by the tumor was measured with a PDT fluorometer (JETI Technische Instrumente GmbH, Jena, Germany) in three different locations on the surface of the skin covering the tumor (excitation 405 nm, emission 550-800 nm). Background fluorescence of intratibial tumor tissue was measured (integration time 7500 ms) in a mouse without PS injection and was subtracted from each measurement resulting in RFU. The mean RFU of the tumor in individual PS-injected mice was calculated from all three emission peak values detected at 652 nm. Upon sacrifice, tumors were cut longitudinally into halves and mTHPC fluorescence was measured inside the tumor tissue in three different locations as described above.

PDT protocol

In both, the xenograft and the syngeneic osteosarcoma model, the mice were randomly assigned to three groups; a control group receiving PS but no illumination (143B/SCID n=10, K7M2L2/BALB/c n=15), a group receiving Foscan-based PDT (143B/SCID n=7, K7M2L2/BALB/c n=8) and a group that was subjected to Foslip-based PDT (143B/SCID n=7, K7M2L2/BALB/c n=9). Foscan or Foslip control mice revealed no difference in any experimental analyses and were therefore merged and presented as one control group (data not shown). A control group of mice that were only illuminated without PS injection was not included here since preliminary studies showed no effect of illumination alone on tumor development (data not shown). Treatment was started after the formation of a tumor (>50 mm^3). Both legs were shaved and the mice were injected with Temgesic (i.p., 0.1 mg/kg). Foscan or Foslip (mTHPC 0.15 mg/kg) were administered by i.v. injection (4-6 min). The mice were kept in a darkened environment for the rest of the experiment. 24 h after mTHPC injection, the mice were

anaesthetized (1-5% isoflurane/O_2) and covered with aluminum foil and black paper such that only the primary tumor within the left hind leg was exposed. The tumors in the PDT groups were illuminated at an energy dose of 20 J/cm^2 (26.817 mW/cm^2, 720 sec) with a 652 nm diode laser (Applied Optronics Corp., South Plainfield, NJ), equipped with a fiber-based frontal light distributor (Medlight SA, Ecublens, Switzerland). Primary tumor growth over time after PDT was monitored by caliper ruler measurements at indicated time points and the data are presented as tumor volume fold-change, comparing the tumor volume in individual mice with the respective volume on the day of PDT.

In the xenograft model (143B/SCID), the mice were sacrificed 14 days after PDT. In the syngeneic model (K7M2L2/BALB/c), three mice per group were sacrificed 2 days after illumination for histological analyses of tumor tissue; all other mice were sacrificed 10 days after PDT.

Pulmonary metastases

After sacrifice of the mice *in situ,* lung perfusion was performed. The lungs were dissected and stained with X-gal for *lacZ*-transduced tumor cells as previously described[32].

Histological analyses in tumor-bearing BALB/c mice

mTHPC fluorescence in primary tumor tissue: Pieces of primary tumor tissue were embedded in mounting medium (Dako, Denmark) and snap frozen in liquid nitrogen. mTHPC in 10 µm sections of primary tumor tissue was visualized with an AxioCam MRm camera connected to a Zeiss Observer.Z1 inverted microscope (Carl Zeiss MicroImaging GmbH) set to 4x magnification and equipped with a fluorescent filter for excitation at 488 nm and detection of emission at 600-700 nm.

Histological stainings: Tumor tissue dissected from the hind-limb at sacrifice was fixed in 4% paraformaldehyde and subsequently decalcified in Osteosoft (Merck Millipore, Germany). The tumors were trimmed, dehydrated in graded alcohol and embedded in paraffin according to standard protocols. Sections of 5-10 µm were mounted on glass slides, deparaffinized in xylene, rehydrated in graded alcohol and stained with hematoxylin and eosin (HE).

Tumor necrosis was assessed in the HE-stained sections as follows: Grade 0: no necrosis; Grade 1: necrosis below 20%; Grade 2: necrosis > 20% and < 40%; Grade 3: necrosis > 40% and < 60%; Grade 4: necrosis > 60% and <80%; Grade 5: necrosis > 80%. Apoptosis was assessed by immunostaining with an antibody to cleaved caspase 3 (Cell Signaling) and tumor vascularization by staining with an antibody to CD31 (Santa Cruz Biotechnologies), a cell surface marker of endothelial cells[33]. The number of apoptotic cells present in tumor sections was normalized to the total number of cells (apoptotic index[34]). Visiomorph software (Visiopharm, Denmark) was employed to calculate the apoptotic index was determined by counting at least 2500 cells in randomly selected areas of tumor tissue sections free of necrosis. Numbers of T (CD3 immunostaining, Spring Biosciences) and B (CD45R immunostaining, BD Biosciences) lymphocytes were counted with the same software in 20 high power fields (HPF) randomly selected in the core and at the periphery of the tumors, avoiding areas of frank necrosis, and in the lungs. Data are presented as the mean (± SEM) number of stained cells/HPF.

Assessment of hind limb blood vessel perfusion

Mice were anesthetized (1-5% isoflurane) and placed in supine position under the laser Doppler perfusion imager (Moor instruments Ltd., UK). Tissue perfusion was measured before PDT and 2, 7 and 10 days after illumination at a speed of 4 ms/pixel using moorLDI Measurement v6.0

software (Moor instruments Ltd., UK). The results were analyzed by drawing a region of interest (ROI) around areas of tumor growth and the corresponding contralateral region in the control limb (normal tissue) using moorLDI Review v6.0. The branching of the epigastric vein from the femoral vein and the branching of the caudal femoral vein were used as anatomical landmarks to define the ROI. The percent difference in perfusion of tumor compared to normal tissue was calculated using the following formula: $(1- (flux_{normal} / flux_{tumor})) \times 100$.

Statistical analysis

In vitro experiments show results of three independent experiments. The results are presented as the mean ± standard error of the mean (SEM) if not described otherwise. Statistical significance of differences between groups was determined using one-way ANOVA with Bonferroni post hoc test. Two-way repeated measures ANOVA with Bonferroni's post-test analysis was used to compare mTHPC uptake *in vitro* and *in vivo* and treatment efficacy (tumor volume, blood vessel perfusion). Statistical analyses were performed using GraphPad Prism Version 5.01 software (GraphPad Software, Inc.). A *P* value below 0.05 was considered to be statistically significant.

Results

Cellular uptake of Foscan and Foslip in osteosarcoma cell lines

In both human 143B and murine K7M2L2 osteosarcoma cells, Foscan and Foslip were taken up in a dose- and time-dependent manner (Figs. 1a, b). No differences in cellular uptake of Foscan and Foslip were observed at mTHPC concentrations up to 10 µg/ml (Fig. 1a). In time course experiments, both the 143B and K7M2L2 cell lines exhibited a slightly delayed uptake of Foslip compared to Foscan, but the difference was no longer significant after 48 h of incubation (Fig. 1b). Confocal laser scanning microscopy of 143B and K7M2L2 cells

incubated with Foscan and Foslip showed a cytoplasmic localization of mTHPC, but no mTHPC in the nucleus (Fig. 1c).

Cytotoxicity of Foscan and Foslip

To investigate differences in photo- and dark-toxicity of Foscan and Foslip in 143B and K7M2L2 osteosarcoma cells, the cells were incubated with the mTHPC formulations at indicated mTHPC concentrations. Foscan exhibited a dose-dependent dark-toxicity in 143B and K7M2L2 cells with half-maximal inhibitory doses (IC_{50}) equivalent to 11.74 µg/ml and 10.4 µg/ml mTHPC, respectively (Fig. 2a). In contrast, Foslip showed no detectable dark-toxicity in both cell lines. Both, Foscan and Foslip showed mTHPC and a laser light dose-dependent phototoxicity (Fig 2b). IC_{50} of Foscan and Foslip in 143B and K7M2L2 cells illuminated with 1 J/cm^2 or 5 J/cm^2 laser light are summarized in Supporting Information Table 1. The data show that the sensitivity of 143B and K7M2L2 cells to Foscan- and Foslip-based PDT was laser light energy dose-dependent and overall comparable.

Both Foscan and Foslip-based treatment induced apoptotic cell death, shown by the presence of cleaved PARP in extracts of cells subjected to PDT in both 143B (Fig. 2c) and K7M2L2 cells (Fig. 2d). In both cell lines, PARP cleavage was suppressed by pretreatment of the cells with the pan-caspase inhibitor Z-VAD-FMK prior to PDT, indicating a caspase dependent apoptosis pathway, confirmed by the detection of cleaved of caspase 3, 7 and 9 in the cell extracts (Supporting Information Figures 1a, b).

***In vivo* uptake of Foslip and Foscan by primary tumors in the xenograft and syngeneic osteosarcoma mouse models**

In order to compare the uptake of the mTHPC formulations Foscan and Foslip by intratibial primary tumors in the xenograft 143B/SCID and the syngeneic K7M2L2/BALB/c osteosarcoma mouse models, the PS formulations were i.v. injected into respective tumor-bearing mice. The uptake by tumor tissue was monitored *in vivo* during 48 h and subsequently analyzed *ex vivo*. In both models, the two mTHPC formulations were taken up by the tumor tissue in a time dependent manner (Figs. 3a, b). In 143B cell line derived tumors, Foslip was taken up significantly more efficiently than Foscan (Fig. 3a), whereas in the K7M2L2 cell line derived tumors, the uptake of Foslip compared to Foscan was only significantly higher at 6 h after PS administration (Fig. 3b). *Ex vivo* measurements of mTHPC fluorescence in dissected tumor and healthy control leg tissue revealed a significant 2.4- and 2.7-times higher uptake of Foscan and Foslip, respectively, in 143B cell line-derived tumors than in the control tissue (Fig. 3c). Similarly, in the K7M2L2/BALB/c model, the uptake of Foscan and Foslip by tumor tissue was 3.4-and 4-times higher, respectively, than by control tissue (Fig. 3d). Based on these *ex vivo* measurements, the uptake of the two mTHPC formulations by tumor tissue was indistinguishable in both osteosarcoma mouse models.

Fluorescence microscopy of tumor tissue cryosections showed a rather uniform distribution of mTHPC fluorescence of Foscan and Foslip in both osteosarcoma mouse models. The fluorescence in adjacent muscle tissue was considerably lower than in tumor tissue in both tumor models indicating again more efficient uptake of both mTHPC formulations by tumor than by healthy tissue (Fig. 3e).

Anti-tumor efficacy of Foscan or Foslip–based PDT in the xenograft and syngeneic osteosarcoma mouse models

We next assessed the tumor suppressive potential of Foscan- and Foslip-based PDT in the two osteosarcoma mouse models. The growth of i.t. tumors derived from 143B cells in SCID mice, lacking functional T and B lymphocytes, was significantly inhibited by Foscan and Foslip-based PDT and Foslip was slightly more effective than Foscan (Figs. 4a, c). Treatment-induced swelling of the tumor leg 3 days after PDT explained the observed transient increase in tumor volume. One week after PDT, the tumor volume of Foslip-treated mice was only 1.2-times and that of Foscan-treated animals only 1.8-times larger compared to the non-treated control mice, which had a 2.2-times larger tumors compared to before PDT. Two weeks after PDT, the tumor volume of the control mice was 4-times larger than before treatment start, whereas mice subjected to Foscan and Foslip-based treatment had only a 2.6-time and 1.8-times, respectively, larger tumors compared to before PDT. The difference in tumor volume in both groups of PDT treated mice was not statistically significant.

In BALB/c mice with an intact immune system, the inhibition of tumor growth by Foscan- and Foslip-mediated PDT was even more pronounced than in SCID mice (Figs. 4b, d). One week after PDT, the tumors in Foscan- or Foslip-based PDT treated mice was indistinguishable and only 2.4 times larger than before treatment compared to the non-treated control mice, which had a 7.8 times larger tumors compared to before PDT. At sacrifice of the mice, K7M2L2 cell line-derived tumors in non-treated mice were 14.3-times larger than at the beginning of the experiment. The tumors of Foscan/PDT treated animals were still only 2.7 times larger and those of Foslip/PDT treated mice only 4.7 times larger than before treatment. In contrast, two days after laser light illumination of the tumor, a swelling and edema formation in the leg where the tumor was localized was observed in all mice subjected to PDT.In the PDT study performed in the KM2L2/BALB/c osteosarcoma model, three mice per

group were sacrificed 48 h after PDT to assess the extent of necrosis and apoptosis in the tumor tissue of treated and non-treated animals (Fig. 4e). Overall, the level of necrosis and apoptosis was remarkably higher in the PDT-treated than in control tumors, which only showed negligible areas of necrosis and cleaved-caspase 3 staining (average necrosis histological score: 0.3; average apoptotic index: 0.02%). Despite variability among the PDT-treated tumors, Foscan/PDT treated tumors exhibited on average higher necrosis (average necrosis histological score: 4.5) and apoptosis (average apoptotic index: 7.5%) scores than those subjected to Foslip- based PDT (average necrosis histological score: 2.7; average apoptotic index: 2.6%).

The effect of Foscan and Foslip - based PDT on pulmonary metastases

To study the impact of the immune system on a putative systemic anti-tumor effect of PDT in experimental osteosarcoma, lungs were dissected at sacrifice from 143B/SCID and from K7M2L2/BALB/c mice 14 and 10 days after Foscan- or Foslip- based PDT. The number of micro- and macrometastases was assessed on the surface of lung whole mounts (Fig. 5 a - c). PDT with either Foscan or Foslip had no effect on pulmonary metastasis in SCID mice (Figs. 5a, c). In contrast, in immunocompetent BALB/c mice, Foscan- and Foslip-based PDT significantly inhibited the formation of lung micro- and macro-metastases to a comparable extent (Figs. 5b, c). Thus, in experimental osteosarcoma investigated here, PDT requires an intact immune system to provoke a systemic anti-tumor effect. In agreement with this, we observed significantly higher numbers of T lymphocytes at the periphery of the tumors in BALB/c mice euthanized 10 days after PDT than in controls (Figure 5 d, f). The number of T lymphocytes in the core of the tumors was only significantly higher in the Foslip treated mice

(Figure e, f). The number of B lymphocytes in the tumors was comparable among the groups (data not shown). Likewise, the numbers of B- or T-lymphocytes within the lungs were not significantly different in the PDT treated and control groups (data not shown).

PDT inhibits tumor perfusion in the syngeneic K7M2L2/BALB/c osteosarcoma mouse model

Blood perfusion of the tumor-bearing and the healthy control hind-limb was measured prior to and after Foscan- and Foslip-based PDT. The perfusion of the tumor-bearing hind limb area before PDT was on average 45.5% higher than in the corresponding hind limb area of the control leg in all experimental groups of mice (Fig. 6a). Two days after PDT, a striking reduction of tumor perfusion was observed in the Foscan- and Foslip-based PDT treated mice ($P < 0.001$). Remarkably, on experimental day 7, the perfusion in the tumors in both treatment groups recovered to levels prior to PDT (Figs. 6.a, b).

The effects of PDT on tumor vascularization were also investigated by histology and immunohistochemistry (Fig. 6c). CD31-immunostained endothelial cells were virtually absent in predominantly necrotic PDT-treated tumor areas, indicating disruption of vessels. In non-necrotic areas of PDT-treated tumors CD31 immunostaining remained detectable, but at overall less density than that observed in tumor tissue not subjected to PDT, which showed moderate to high numbers of CD31-stained blood vessels.

Discussion

This study investigated the potential use of PDT in two clinically relevant models of experimental

osteosarcoma as a novel approach for effective treatment of metastasizing osteosarcoma. The study compared the uptake and dark- and phototoxicity *in vitro* and the efficacy of PDT *in vivo* with mTHPC in the free formulation Foscan and the liposomal formulation Foslip. It took advantage of the orthotopic human 143B and the mouse K7M2L2 cell line, which form primary intratibial tumors and lung metastases within two weeks after inoculation in immune-defective SCID and in syngeneic immune-competent BALB/c mice, respectively.

The results of the experiments carried out *in vitro*, demonstrating comparable time- and dose-dependent uptake of both Foscan and Foslip in the two osteosarcoma cell lines, are in line with the results of previous studies performed in human biliary cancer cell lines[35]. Despite a slightly less efficient uptake of Foslip compared to Foscan by the two osteosarcoma cell lines over time, both compounds showed a comparable phototoxicity triggering apoptosis, but importantly, Foslip, unlike Foscan, showed hardly any dark-toxicity at the concentrations used in the present study. This later finding was again in good agreement with those of the study with the human biliary cancer cell lines[35] due to the considerable toxicity of ethanol/propandiol (data not shown), which is used as a solvent for Foscan in place of water for Foslip.

Crucial for the success of PDT in cancer therapy is a predominant uptake of PS by tumor compared to healthy tissue. This was indeed observed *in vivo* and *ex vivo* for i.v. administered Foscan and Foslip in both osteosarcoma mouse models investigated in the present study. These results confirmed a previously reported higher content of both formulations in tumor than in adjacent muscle tissue[27, 36]. Two mechanisms have been proposed to account for these findings. Both Foscan and Foslip bind to serum proteins such as albumin and high and low density lipoproteins (HDL/LDL) that facilitate their cellular uptake, which is apparently accelerated in fast proliferating cancer cells that are dependent on a high transport rate of lipoproteins[37, 38]. Increased

PS uptake in tumor compared to healthy tissue is also caused by anatomical changes within the tumor, characterized by an enhanced leakiness of tumor blood vessels, and a slower lymphatic drainage, causing an accumulation of the PS in the tumor tissue, called the enhanced permeability and retention (EPR) effect[39, 40].

The results of the here reported experiments, analyzing the time-dependent uptake of mTHPC by tumor tissue, showed a significantly higher uptake of Foslip than of Foscan at all time points investigated in the 143B/SCID model and at 6 hours after mTHPC administration in the K7M2L2/BALB/c model. These observations are consistent with the findings of De Visscher *et al*., who reported a significantly higher increase of Foslip than of Foscan fluorescence intensities upon i.v. PS administration in a subcutaneous adenocarcinoma mouse model[41]. Thus, Foslip appears to enhance the bioavailability of mTHPC in tumor tissue. Along these lines, it is assumed that liposomal carriers enhance the EPR effect due to the formation of larger macromolecules upon binding to plasma proteins[42, 43].

Already 20 years ago, pioneering studies performed by Korbelik *et al*., demonstrated the importance of an intact immune system for the efficacy of PDT[44]. A comparison of the efficacy of PDT in immune-compromised and in immune-competent mice in the present study confirmed the important findings of Korbelik *et al*. PDT with Foscan and Foslip only transiently inhibited the growth of intratibial 143B cell line-derived tumors in SCID mice and had no significant effect on lung metastasis. In immune-competent BALB/c mice, however, the growth of K7M2L2 cell line-derived primary tumors was persistently suppressed and the formation of both micro- and macro-metastases significantly inhibited by PDT with the two PS formulations. Additionally, our findings indicate increased infiltration of T-lymphocytes at the primary tumor site, pointing to a PDT activated T cell adaptive immunity that decreases pulmonary metastasis. Altogether, the findings

confirmed the important impact of an intact immune system on PDT efficacy reported by Korbelik *et al*. and needs to be further explored.

Due to enhanced angiogenesis in the tumor bearing leg, blood flow was significantly enhanced in all groups of mice before photodynamic treatment. Analysis of tumor vascularization and perfusion in the K7M2L2/BALB/c model demonstrated a pronounced inhibitory effect of the PDT on the blood supply of the primary tumor. These observations are consistent with reported toxic and inhibitory effects of PDT on endothelial cells and platelet formation, respectively, leading to vascular leakage and collapse and, consequently, an impaired blood flow in the treated tumor bearing leg [11, 45, 46]. However, this effect was only temporary, likely due to compensatory mechanisms in non-damaged neighboring blood vessels that restored the blood flow to levels before treatment. Since angiogenesis plays a major role in tumor progression, targeting tumor vascularization by PDT has an additional at least transient beneficial tumor suppressive effect[47].

Interestingly, in the 143B/SCID model, Foslip was more effective than Foscan, presumably due to the observed higher amounts of mTHPC accumulating in tumors of Foslip than of Foscan-treated mice and to previously reported higher concentrations of monomeric mTHPC achieved with liposomal formulations, as hydrophobic PS (Foscan) strongly aggregate in aqueous media weakening their photosensitizing efficacy[37, 42].

Differences in efficacy between Foscan- based and Foslip-based PDT was only observed in the xenograft mouse model, further studies are needed to evaluate additional treatment setting for both mTHPC formulations. The relation of the liposomal carrier system and their pharmacokinetics to PDT efficacy is still under debate. Previous studies in preclinical mammary carcinoma and fibrosarcoma models showed no correlation of the PS concentrations in the tumor and PDT efficacy, indicating a correlation between PDT efficacy and PS concentration in

endothelial cells [48, 49]. On the other side, d`Hallewin *et al*. demonstrated the importance of Foslip accumulation in the tumor tissue, giving rise to the highest amount of tumor necrosis with the highest PS concentration in the tumor[50]. Our results provide a first hint that in osteosarcoma, Foslip is equally potent compared to Foscan, but to truly compare the PDT efficiency between both compounds, further studies are needed.

In summary, this study demonstrates potent mTHPC-based PDT-mediated tumor suppressive effects in two clinically relevant intratibial mouse models of osteosarcoma, and clearly demonstrates the potential of PDT to inhibit lung metastatic growth in animals with an intact immune system. Considering that PDT has a relatively low systemic toxicity, repetitive application is possible. Consequently, it is an interesting novel option for the treatment of osteosarcoma, even in combination with current standards of care including neoadjuvant chemotherapy.

Acknowledgments

The authors thank Matthias JE Arlt for his help with intratibial injections of tumor cells and Tojo Razafiarison for confocal microscopy and statistical analysis. Our work was supported by the University of Zurich, the Schweizerischer Verein Balgrist (Zurich, Switzerland), the Walter L. & Johanna Wolf Foundation (Zurich, Switzerland), the Highly Specialized Medicine for Musculoskeletal Oncology program of the Canton of Zurich, the Zurcher Krebsliga (Zurich, Switzerland), the Swiss National Science Foundation SNF Nr.310030_149649 and the EuroNanoMed ERA-NET grant.

References

1. Rainusso N, Wang LL, Yustein JT. The adolescent and young adult with cancer: state of the art -- bone tumors. Curr Oncol Rep 2013;15:296-307.

2. Ward E, DeSantis C, Robbins A, Kohler B, Jemal A. Childhood and adolescent cancer statistics, 2014. CA Cancer J Clin 2014;64:83-103.

3. Mirabello L, Troisi RJ, Savage SA. Osteosarcoma incidence and survival rates from 1973 to 2004: data from the Surveillance, Epidemiology, and End Results Program. Cancer 2009;115:1531-43.

4. Allison DC, Carney SC, Ahlmann ER, Hendifar A, Chawla S, Fedenko A, Angeles C, Menendez LR. A meta-analysis of osteosarcoma outcomes in the modern medical era. Sarcoma 2012;2012:704872.

5. Miller BJ, Cram P, Lynch CF, Buckwalter JA. Risk factors for metastatic disease at presentation with osteosarcoma: an analysis of the SEER database. J Bone Joint Surg Am 2013;95:e89.

6. Whelan JS, Bielack SS, Marina N, Smeland S, Jovic G, Hook JM, Krailo M, Anninga J, Butterfass-Bahloul T, Bohling T, Calaminus G, Capra M, et al. EURAMOS-1, an international randomised study for osteosarcoma: results from pre-randomisation treatment. Annals of oncology : official journal of the European Society for Medical Oncology / ESMO 2015;26:407-14.

7. Janeway KA, Grier HE. Sequelae of osteosarcoma medical therapy: a review of rare acute toxicities and late effects. Lancet Oncol 2010;11:670-8.

8. He H, Ni J, Huang J. Molecular mechanisms of chemoresistance in osteosarcoma (Review). Oncol Lett 2014;7:1352-62.

9. Botter SM, Neri D, Fuchs B. Recent advances in osteosarcoma. Curr Opin Pharmacol 2014;16:15-23.

10. Fayter D, Corbett M, Heirs M, Fox D, Eastwood A. A systematic review of photodynamic therapy in the treatment of pre-cancerous skin conditions, Barrett's oesophagus and cancers of the biliary tract, brain, head and neck, lung, oesophagus and skin. Health Technol Assess 2010;14:1-288.

11. Agostinis P, Berg K, Cengel KA, Foster TH, Girotti AW, Gollnick SO, Hahn SM, Hamblin MR, Juzeniene A, Kessel D, Korbelik M, Moan J, et al. Photodynamic therapy of cancer: an update. CA Cancer J Clin 2011;61:250-81.

12. Zhang X, Liu T, Li Z. Progress of photodynamic therapy applications in the treatment of musculoskeletal sarcoma (Review). Oncol Lett 2014;8:1403-8.

13. Usuda J, Kato H, Okunaka T, Furukawa K, Tsutsui H, Yamada K, Suga Y, Honda H, Nagatsuka Y, Ohira T, Tsuboi M, Hirano T. Photodynamic therapy (PDT) for lung cancers. J Thorac Oncol 2006;1:489-93.

14. Gomer CJ, Ferrario A, Murphree AL. The effect of localized porphyrin photodynamic therapy on the induction of tumour metastasis. Br J Cancer 1987;56:27-32.

15. Kabingu E, Oseroff AR, Wilding GE, Gollnick SO. Enhanced systemic immune reactivity to a Basal cell carcinoma associated antigen following photodynamic therapy. Clin Cancer Res 2009;15:4460-6.

16. Thong PS, Ong KW, Goh NS, Kho KW, Manivasager V, Bhuvaneswari R, Olivo M, Soo KC. Photodynamic-therapy-activated immune response against distant untreated tumours in recurrent angiosarcoma. Lancet Oncol 2007;8:950-2.

17. Lorenz KJ, Maier H. Photodynamic therapy with meta-tetrahydroxyphenylchlorin (Foscan) in the management of squamous cell carcinoma of the head and neck: experience with 35 patients. Eur Arch Otorhinolaryngol 2009;266:1937-44.

18. Bredell MG, Besic E, Maake C, Walt H. The application and challenges of clinical PD-PDT in the head and neck region: a short review. J Photochem Photobiol B 2010;101:185-90.

19. Reidy K, Campanile C, Muff R, Born W, Fuchs B. mTHPC-Mediated Photodynamic Therapy is Effective in the Metastatic Human 143B Osteosarcoma Cells. Photochem Photobiol 2012;88:721-7.

20. Kusuzaki K, Minami G, Takeshita H, Murata H, Hashiguchi S, Nozaki T, Ashihara T, Hirasawa Y. Photodynamic inactivation with acridine orange on a multidrug-resistant mouse osteosarcoma cell line. Jpn J Cancer Res 2000;91:439-45.

21. Yanase S, Nomura J, Matsumura Y, Watanabe Y, Tagawa T. Synergistic increase in osteosarcoma cell sensitivity to photodynamic therapy with aminolevulinic acid hexyl ester in the presence of hyperthermia. Photomed Laser Surg 2009;27:791-7.

22. Meier D, Campanile C, Botter SM, Born W, Fuchs B. Cytotoxic efficacy of photodynamic therapy in osteosarcoma cells in vitro. J Vis Exp 2014;85.

23. Nomura J, Yanase S, Matsumura Y, Nagai K, Tagawa T. Efficacy of combined photodynamic and hyperthermic therapy with a new light source in an in vivo osteosarcoma tumor model. J Clin Laser Med Surg 2004;22:3-8.

24. Sun M, Zhou C, Zeng H, Puebla-Osorio N, Damiani E, Chen J, Wang H, Li G, Yin F, Shan L, Zuo D, Liao Y, et al. Hiporfin-Mediated Photodynamic Therapy in Preclinical Treatment of Osteosarcoma. Photochem Photobiol 2015;91:533–44

25. Burch S, London C, Seguin B, Rodriguez C, Wilson BC, Bisland SK. Treatment of canine osseous tumors with photodynamic therapy: a pilot study. Clin Orthop Relat Res 2009;467:1028-34.

26. Buchholz J, Wergin M, Walt H, Grafe S, Bley CR, Kaser-Hotz B. Photodynamic therapy of feline cutaneous squamous cell carcinoma using a newly developed liposomal photosensitizer: preliminary results concerning drug safety and efficacy. J Vet Intern Med 2007;21:770-5.

27. Reshetov V, Lassalle HP, Francois A, Dumas D, Hupont S, Grafe S, Filipe V, Jiskoot W, Guillemin F, Zorin V, Bezdetnaya L. Photodynamic therapy with conventional and

PEGylated liposomal formulations of mTHPC (temoporfin): comparison of treatment efficacy and distribution characteristics in vivo. Int J Nanomedicine 2013;8:3817-31.

28. Reshetov V, Kachatkou D, Shmigol T, Zorin V, D'Hallewin MA, Guillemin F, Bezdetnaya L. Redistribution of meta-tetra(hydroxyphenyl)chlorin (m-THPC) from conventional and PEGylated liposomes to biological substrates. Photochem Photobiol Sci 2011;10:911-9.

29. Arlt MJ, Banke IJ, Walters DK, Puskas GJ, Steinmann P, Muff R, Born W, Fuchs B. LacZ transgene expression in the subcutaneous Dunn/LM8 osteosarcoma mouse model allows for the identification of micrometastasis. J Orthop Res 2011;29:938-46.

30. Sabile AA, Arlt MJ, Muff R, Bode B, Langsam B, Bertz J, Jentzsch T, Puskas GJ, Born W, Fuchs B. Cyr61 expression in Osteosarcoma indicates poor prognosis and promotes intratibial growth and lung metastasis in mice. J Bone Miner Res 2011;27:58-67.

31. Fidler IJ, Naito S, Pathak S. Orthotopic implantation is essential for the selection, growth and metastasis of human renal cell cancer in nude mice [corrected]. Cancer Metastasis Rev 1990;9:149-65.

32. Arlt MJ, Born W, Fuchs B. Improved Visualization of Lung Metastases at Single Cell Resolution in Mice by Combined In-situ Perfusion of Lung Tissue and X-Gal Staining of lacZ-Tagged Tumor Cells. J Vis Exp 2012.

33. Wang D, Stockard CR, Harkins L, Lott P, Salih C, Yuan K, Buchsbaum D, Hashim A, Zayzafoon M, Hardy RW, Hameed O, Grizzle W, et al. Immunohistochemistry in the evaluation of neovascularization in tumor xenografts. Biotech Histochem 2008;83:179-89.

34. Bressenot A, Marchal S, Bezdetnaya L, Garrier J, Guillemin F, Plenat F. Assessment of apoptosis by immunohistochemistry to active caspase-3, active caspase-7, or cleaved PARP in monolayer cells and spheroid and subcutaneous xenografts of human carcinoma. J Histochem Cytochem 2009;57:289-300.

35. Kiesslich T, Berlanda J, Plaetzer K, Krammer B, Berr F. Comparative characterization of the efficiency and cellular pharmacokinetics of Foscan- and Foslip-based photodynamic treatment in human biliary tract cancer cell lines. Photochem Photobiol Sci 2007;6:619-27.

36. Svensson J, Johansson A, Grafe S, Gitter B, Trebst T, Bendsoe N, Andersson-Engels S, Svanberg K. Tumor selectivity at short times following systemic administration of a liposomal temoporfin formulation in a murine tumor model. Photochem Photobiol 2007;83:1211-9.

37. Reshetov V, Zorin V, Siupa A, D'Hallewin MA, Guillemin F, Bezdetnaya L. Interaction of liposomal formulations of meta-tetra(hydroxyphenyl)chlorin (temoporfin) with serum proteins: protein binding and liposome destruction. Photochem Photobiol 2012;88:1256-64.

38. Guo D, Bell EH, Mischel P, Chakravarti A. Targeting SREBP-1-driven lipid metabolism to treat cancer. Curr Pharm Des 2014;20:2619-26.

39. Fang J, Nakamura H, Maeda H. The EPR effect: Unique features of tumor blood vessels for drug delivery, factors involved, and limitations and augmentation of the effect. Adv Drug Deliv Rev 2011;63:136-51.

40. Greish K. Enhanced permeability and retention of macromolecular drugs in solid tumors: a royal gate for targeted anticancer nanomedicines. J Drug Target 2007;15:457-64.

41. de Visscher SA, Kascakova S, de Bruijn HS, van den Heuvel A, Amelink A, Sterenborg HJ, Robinson DJ, Roodenburg JL, Witjes MJ. Fluorescence localization and kinetics of mTHPC and liposomal formulations of mTHPC in the window-chamber tumor model. Lasers Surg Med 2011;43:528-36.

42. Derycke AS, de Witte PA. Liposomes for photodynamic therapy. Adv Drug Deliv Rev 2004;56:17-30.

43. Konan YN, Gurny R, Allemann E. State of the art in the delivery of photosensitizers for photodynamic therapy. J Photochem Photobiol B 2002;66:89-106.

44. Korbelik M, Krosl G, Krosl J, Dougherty GJ. The role of host lymphoid populations in the response of mouse EMT6 tumor to photodynamic therapy. Cancer Res 1996;56:5647-52.

45. Gomer CJ, Rucker N, Murphree AL. Differential cell photosensitivity following porphyrin photodynamic therapy. Cancer Res 1988;48:4539-42.

46. Star WM, Marijnissen HP, van den Berg-Blok AE, Versteeg JA, Franken KA, Reinhold HS. Destruction of rat mammary tumor and normal tissue microcirculation by hematoporphyrin derivative photoradiation observed in vivo in sandwich observation chambers. Cancer Res 1986;46:2532-40.

47. Bergers G, Benjamin LE. Tumorigenesis and the angiogenic switch. Nat Rev Cancer 2003;3:401-10.

48. Jones HJ, Vernon DI, Brown SB. Photodynamic therapy effect of m-THPC (Foscan) in vivo: correlation with pharmacokinetics. Br J Cancer 2003;89:398-404.

49. Lassalle HP, Dumas D, Grafe S, D'Hallewin MA, Guillemin F, Bezdetnaya L. Correlation between in vivo pharmacokinetics, intratumoral distribution and photodynamic efficiency of liposomal mTHPC. J Control Release 2009;134:118-24.

50. D'Hallewin MA, Kochetkov D, Viry-Babel Y, Leroux A, Werkmeister E, Dumas D, Grafe S, Zorin V, Guillemin F, Bezdetnaya L. Photodynamic therapy with intratumoral administration of Lipid-Based mTHPC in a model of breast cancer recurrence. Lasers Surg Med 2008;40:543-9.

Figure Legends

Figure 1. Dose- and time-dependent uptake of Foscan and Foslip in 143B and K7M2L2 osteosarcoma cells. Cells were incubated in the dark with either Foscan (■) or Foslip (●) with the indicated concentrations of mTHPC for 5 h (a) or with 2.5 μg/ml mTHPC for indicated time periods (b). After washing with PBS, mTHPC fluorescence intensity (indicated as relative fluorescence unit (RFU)) was measured at 652 nm after excitation at 452 nm. * $P < 0.05$, ** $P < 0.01$, Foscan compared with Foslip. (c) Representative images of cellular localization of mTHPC by confocal laser scanning microscopy in 143B and K7M2L2 cells. mTHPC fluorescence appeared red and nuclei stained with Hoechst appeared blue, 20-fold magnification, scale bar, 100 μm.

Figure 2. Dark- and photo-toxicity of Foscan and Foslip in 143B and K7M2L2 osteosarcoma cells, and PDT induced apoptosis. (a) Dose-dependent dark-toxicity. 143B (left panel) and K7M2L2 (right panel) cells (2000 cells/ well) were incubated in the dark in the absence (control, set to 100%) or in the presence of indicated concentrations of mTHPC (Foscan ■, Foslip ●) for 5 h. Cell viability was assessed in a WST-1 assay. (b) Dose-dependent photo-toxicity. 143B (left panel) and K7M2L2 (right panel) cells (800 cells/ well) were incubated in the dark in the absence (control, set to 100%) or in the presence of indicated concentrations of mTHPC for 5 h and subsequently illuminated with doses of 1 J/cm^2 (Foscan □, Foslip ○) or 5 J/cm^2 (Foscan ■, Foslip ●) of 652 nm laser light. The cell viability was determined as in (a). (c) Inhibition of PDT-induced PARP cleavage by Z-VAD-FMK in 143B cells. The cells were pre-incubated in the absence or presence of Z-VAD-FMK or DMSO and treated with Foscan (left panel) or Foslip (right panel) at indicated concentrations and subjected to PDT as

described in Materials and Methods. (d) Inhibition of PARP cleavage by Z-VAD-FMK in K7M2L2 subjected to PDT as described in (c). GAPDH was used as protein loading controls.

Figure 3. Uptake of Foscan or Foslip by intratibial human xenograft 143B cell line-derived tumors in SCID mice and by intratibial mouse K7M2L2 cell line-derived tumors in syngeneic BALB/c mice. SCID and BALB/c mice with tumors > 50 mm^3 were i.v. injected with Foscan or Foslip equivalent to 1.5 mg/kg mTHPC and the uptake of the mTHPC formulations by tumor tissue over time was assessed with a fluorimeter as described in Materials and Methods. Fluorescence measurements were corrected for background fluorescence of tumor tissue, assessed in non-injected mice (no mTHPC). (a) Mean (± SEM) uptake (indicated as RFU) *in vivo* of listed mTHPC formulations at indicated time points by 143B cell line-derived tumors (n=10) and (b) by K7M2L2 cell line-derived tumors (n=14). .* $P < 0.05$, ** $P < 0.01$, *** $P < 0.001$ Foslip compared to Foscan (2-way ANOVA, Bonferroni post-test). (c) Mean (± SEM) uptake (RFU) of indicated formulations assessed *ex vivo* 48 h after PS injection in 143B cell line-derived tumors (n=10) and in corresponding healthy leg tissue (control leg) and (d) in K7M2L2 cell line-derived tumors (n=14) and in control legs. * $P < 0.05$, ** $P < 0.01$, *** $P < 0.001$ tumor leg compared to control leg, n.s.: not significant (1-way ANOVA, Bonferroni post-test). (e) *Ex vivo* visualization of mTHPC (red) in cryosections (fluorescence filter ~620nm) of primary tumor tissue of Foscan- or Foslip- and non-injected mice. White arrows point to muscle fibers surrounded by tumor tissue. Scale bar, 200 μm.

Figure 4. Inhibition of osteosarcoma primary tumor growth in two intratibial osteosarcoma mouse models in response to Foscan or Foslip based PDT (i.v. PS administration equivalent to 0.15 mg/kg mTHPC, 20 J/cm^2). (a) Mean (± SEM) fold change in size of intratibial human

143B cell line-derived tumors in SCID mice (10 control, 7 Foscan and 7 Foslip-treated mice) and (b) of intratibial mouse K7M2L2 cell line-derived tumors in syngeneic BALB/c mice (15 control, 8 Foscan and 9 Foslip-treated mice) assessed on indicated days after PDT by caliper measurements and normalized to the tumor size in individual mice measured on the day of PDT treatment. The control groups of mice received PS but no laser light illumination (control). (c) Photographs taken on day of PDT and at the end of treatment study from representative SCID mice with intratibial 143B cell line-derived tumors and (d) from representative BALB/c mice with intratibial K7M2L2 cell line-derived tumors in the right hind limb. The mice were treated as indicated. + $P < 0.05$, +++ $P < 0.001$ Foscan PDT vs. control, *** $P < 0.001$ Foslip PDT vs. control. Dotted lines indicate tumor areas. (e) Representative images of 5 μm sections of K7M2L2 cell line-derived intratibial tumors collected two days after PDT from BALB/c mice treated as indicated. The sections were stained with hematoxylin and eosin (HE) for histological examination and immunostained for cleaved caspase 3 (CC3) indicating apoptotic tissue areas. N: necrosis, V: viable tumor, black arrows indicate apoptotic cells. Scale bars: top panel, 1 mm, bottom panel, 100 μm.

Figure 5. Effect of intratibial primary tumor treatment by PDT on pulmonary metastases and immune cell infiltration. (a) *Ex vivo* quantification of X-Gal stained 143B/*LacZ* cell-derived metastases on the surface of whole mounts of lungs collected from SCID mice at sacrifice 14 days after PDT. The data indicate the numbers of pulmonary micrometastases per lung (diameter < 0.1mm, left panel) and of pulmonary macrometastases (diameter > 0.1mm, right panel) in individual mice of the indicated treatment groups. The numbers of lungs analyzed in the different experimental groups are shown by the number of corresponding symbols in the

figures. (b) *Ex vivo* quantification of X-Gal stained K7M2L2/*LacZ* cells on whole mounts of lungs collected from BALB/c mice at sacrifice 10 days after treatment. Data analysis as described in (a). (c) Representative images of X-gal–stained metastatic nodules on whole mounts of lungs of SCID mice and BALB/c mice. Black arrows point to pulmonary micrometastases and the open black arrow to a macrometastasis. Scale bar, 200 μm. (d) Mean (± SEM) number of T-lymphocytes per high power field (HPF) in primary tumor periphery. (e) Mean (± SEM) number of T-lymphocytes per high power field (HPF) in primary tumor core. (f) Representative images of H&E stained 5 μm sections of intratibial tumors collected 10 days after PDT from BALB/c mice treated as indicated. T-lymphocytes were identified by immunohistochemistry for the CD3 antigen (arrows) in the core (red rectangle) and at the periphery (green rectangle) of the tumors. V: viable tumor tissue, N: necrotic tumor tissue, pln: popliteal lymph node (on slide positive tissue control), *: soft tissue adjacent to the tumor. Scale bars: low magnification panel, 5 mm, high magnification panels, 50 μm. * $P < 0.05$, ** $P < 0.01$, *** $P < 0.001$, PDT-treated groups vs. control, n.s.: not significant.

Figure 6. Effect of primary tumor treatment by Foscan or Foslip-based PDT on hind limb blood flow in the syngeneic K7M2L2/BALB/c osteosarcoma mouse model. (a) Blood flow in control and tumor-bearing hind limbs was measured with a laser Doppler perfusion imager in the regions of interest (ROI) (as indicated in b), and the data collected from 12 mice per treatment group on indicated experimental days are presented as percent change in perfusion (flux) of tumor compared to normal tissue, *** $P < 0.001$ PDT- treated vs. control. (b) Images of hind limb perfusion taken on indicated experimental days from representative mice of the

different experimental groups. White circles indicate ROI for laser Doppler image analysis. (c) Representative images of CD31 immunostained 10 μm sections of intratibial tumors collected from representative mice of the indicated treatment groups on day 2 after PDT. Black arrows point to CD31-stained endothelial cells, scale bar 250 μm.

Supporting Information Table 1. Half-maximal cell viability inhibitory doses (IC_{50}) of Foscan and Foslip in 143B and K7M2L2 osteosarcoma cells subjected to PDT with light energy doses of 1J/cm^2 or 5 J/cm^2 as indicated.

Supporting Information Figure 1. 10^6 143B (a) or K7M2L2 (b) cells were incubated for 5 h with Foscan or Foslip at indicated mTHPC concentrations. Osteosarcoma cells were illuminated (as described in Material and Methods) or kept in the dark. Cell lysates were analyzed with antibodies to cleaved caspase 3 (1:1000, Cell Signaling Technology, Danvers, MA), to cleaved caspase 7 (1:1000, Cell Signaling Technology), to caspase 9 and cleaved caspase 9 (1:1000, Cell Signaling Technology), to PARP and cleaved PARP (1:1000, Cell Signaling Technology), to GAPDH (1:3000 Santa Cruz Biotechnologies) and to Actin (1:10`000, Millipore Darmstadt, Germany). GAPDH and Actin were used as protein loading controls.

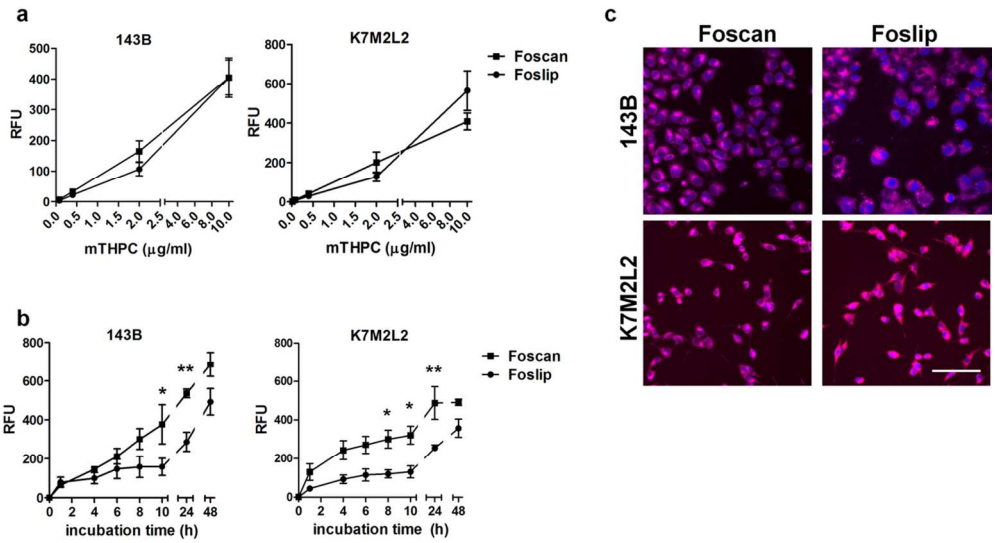

Figure 1. Dose- and time-dependent uptake of Foscan and Foslip in 143B and K7M2L2 osteosarcoma cells. Cells were incubated in the dark with either Foscan (■) or Foslip (●) with the indicated concentrations of mTHPC for 5 h (a) or with 0.6 µg/ml mTHPC for indicated time periods (b). After washing with PBS, mTHPC fluorescence intensity (indicated as relative fluorescence unit (RFU)) was measured at 652 nm after excitation at 452 nm. * $P < 0.05$, ** $P < 0.01$, Foscan compared with Foslip. (c) Representative images of cellular localization of mTHPC by confocal laser scanning microscopy in 143B and K7M2L2 cells. mTHPC fluorescence appeared red and nuclei stained with Hoechst appeared blue, 20-fold magnification, scale bar, 100 µm.

113x62mm (300 x 300 DPI)

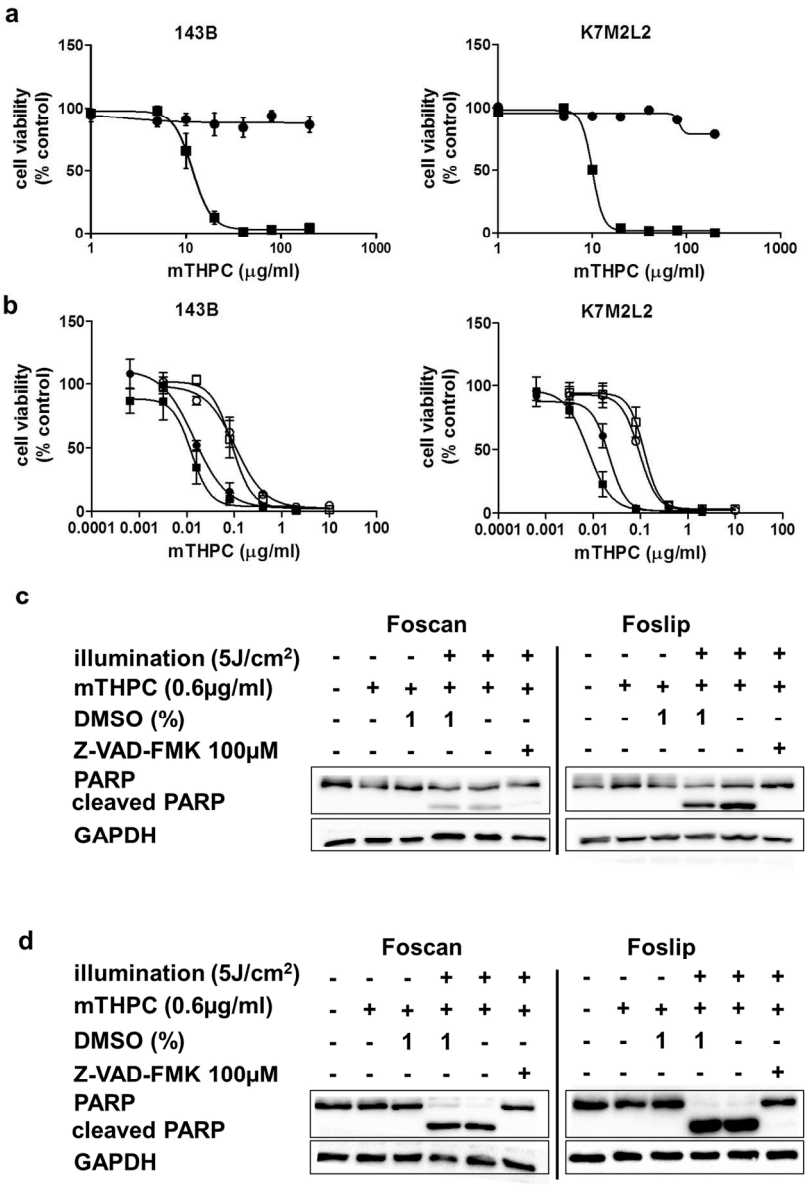

Figure 2. Dark- and photo-toxicity of Foscan and Foslip in 143B and K7M2L2 osteosarcoma cells, and PDT induced apoptosis. (a) Dose-dependent dark-toxicity. 143B (left panel) and K7M2L2 (right panel) cells (2000 cells/ well) were incubated in the dark in the absence (control, set to 100%) or in the presence of indicated concentrations of mTHPC (Foscan ■, Foslip ●) for 5 h. Cell viability was assessed in a WST-1 assay. (b) Dose-dependent photo-toxicity. 143B (left panel) and K7M2L2 (right panel) cells (800 cells/ well) were incubated in the dark in the absence (control, set to 100%) or in the presence of indicated concentrations of mTHPC for 5 h and subsequently illuminated with doses of 1 J/cm^2 (Foscan □, Foslip ○) or 5 J/cm^2 (Foscan ■, Foslip ●) of 652 nm laser light. The cell viability was determined as in (a). (c) Inhibition of PDT-induced PARP cleavage by Z-VAD-FMK in 143B cells. The cells were pre-incubated in the absence or presence of Z-VAD-FMK or DMSO and treated with Foscan (left panel) or Foslip (right panel) at indicated concentrations and subjected to PDT as described in Materials and Methods. (d) Inhibition of PARP cleavage by Z-VAD-FMK in K7M2L2 subjected to PDT as described in (c). GAPDH was used as protein loading controls.

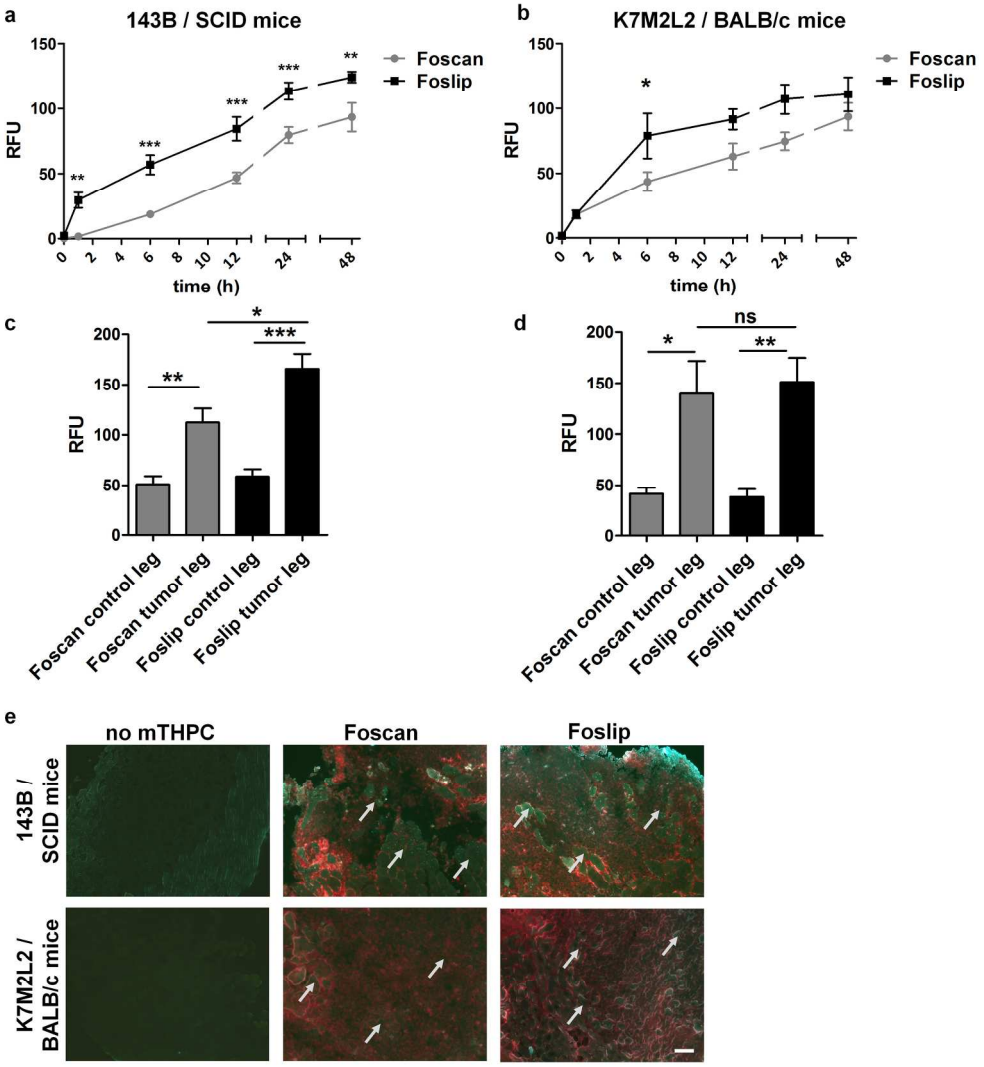

Figure 3. Uptake of Foscan or Foslip by intratibial human xenograft 143B cell line-derived tumors in SCID mice and by intratibial mouse K7M2L2 cell line-derived tumors in syngeneic BALB/c mice. SCID and BALB/c mice with tumors > 50 mm^3 were i.v. injected with Foscan or Foslip equivalent to 1.5 mg/kg mTHPC and the uptake of the mTHPC formulations by tumor tissue over time was assessed with a fluorimeter as described in Materials and Methods. Fluorescence measurements were corrected for background fluorescence of tumor tissue, assessed in non-injected mice (no mTHPC). (a) Mean (± SEM) uptake (indicated as RFU) in vivo of listed mTHPC formulations at indicated time points by 143B cell line-derived tumors (n=10) and (b) by K7M2L2 cell line-derived tumors (n=14). .* $P < 0.05$, ** $P < 0.01$, *** $P < 0.001$ Foslip compared to Foscan (2-way ANOVA, Bonferroni post-test). (c) Mean (± SEM) uptake (RFU) of indicated formulations assessed *ex vivo* 48 h after PS injection in 143B cell line-derived tumors (n=10) and in corresponding healthy leg tissue (control leg) and (d) in K7M2L2 cell line-derived tumors (n=14) and in control legs. * $P < 0.05$, ** $P < 0.01$, *** $P < 0.001$ tumor leg compared to control leg, n.s.: not significant (1-way ANOVA, Bonferroni post-test). (e) *Ex vivo* visualization of mTHPC (red) in cryosections (fluorescence filter ~620nm) of indicated primary tumor tissue of Foscan- or Foslip- and non-injected mice. White arrows point to muscle fibers surrounded by tumor tissue. Scale bar, 200 µm.

220x239mm (300 x 300 DPI)

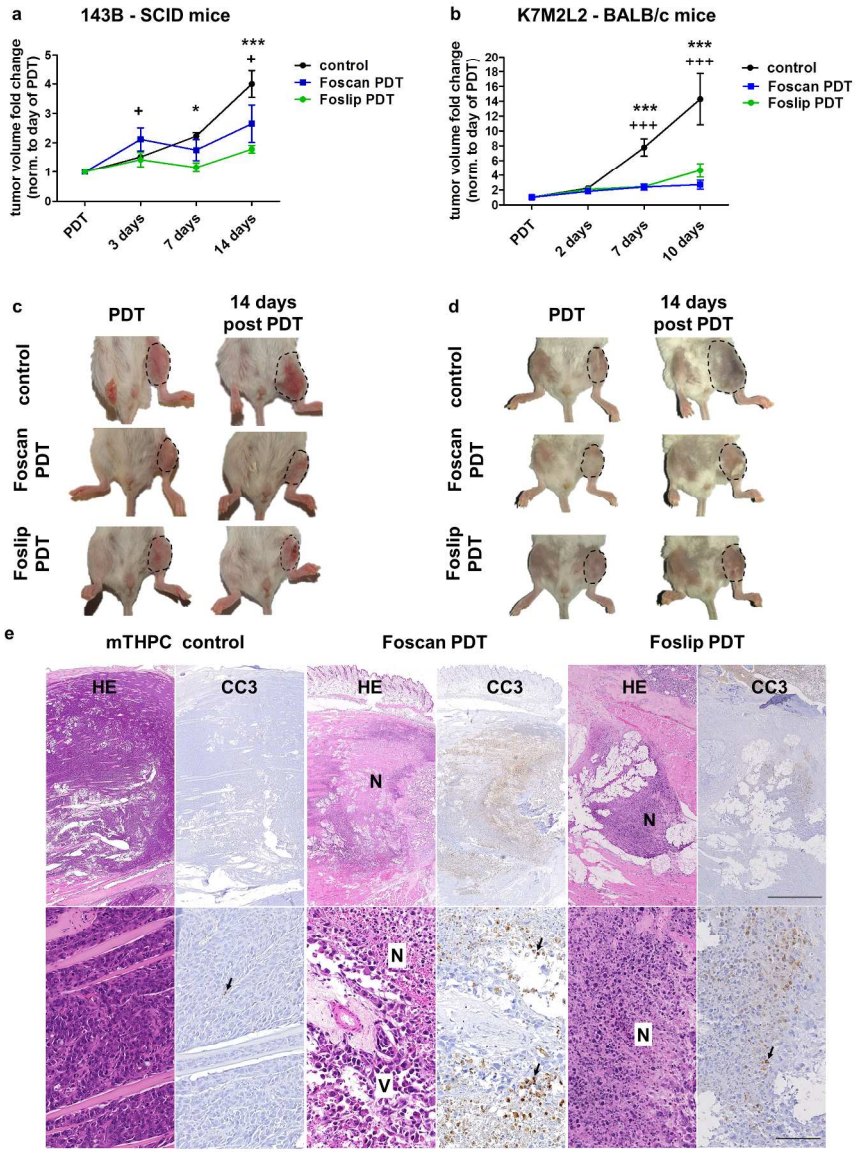

Figure 4. Inhibition of osteosarcoma primary tumor growth in two intratibial osteosarcoma mouse models in response to Foscan or Foslip based PDT (i.v. PS administration equivalent to 0.15 mg/kg mTHPC, 20 J/cm2). (a) Mean (± SEM) fold change in size of intratibial human 143B cell line-derived tumors in SCID mice (10 control, 7 Foscan and 7 Foslip-treated mice) and (b) of intratibial mouse K7M2L2 cell line-derived tumors in syngeneic BALB/c mice (15 control, 8 Foscan and 9 Foslip-treated mice) assessed on indicated days after PDT by caliper measurements and normalized to the tumor size in individual mice measured on the day of PDT treatment. The control groups of mice received PS but no laser light illumination (control). (c) Photographs taken on day of PDT and at the end of treatment study from representative SCID mice with intratibial 143B cell line-derived tumors and (d) from representative BALB/c mice with intratibial K7M2L2 cell line-derived tumors in the right hind limb. The mice were treated as indicated. + $P < 0.05$, +++ $P < 0.001$ Foscan PDT vs. control, *** $P < 0.001$ Foslip PDT vs. control. Dotted lines indicate tumor areas. (e) Representative images of 5 µm sections of K7M2L2 cell line-derived intratibial tumors collected two days after PDT from BALB/c mice treated as indicated. The sections were stained with hematoxylin and eosin (HE)

for histological examination and immunostained for cleaved caspase 3 (CC3) indicating apoptotic tissue areas. N: necrosis, V: viable tumor, black arrows indicate apoptotic cells. Scale bars: top panel, 1 mm, bottom panel, 100 µm.

338x431mm (300 x 300 DPI)

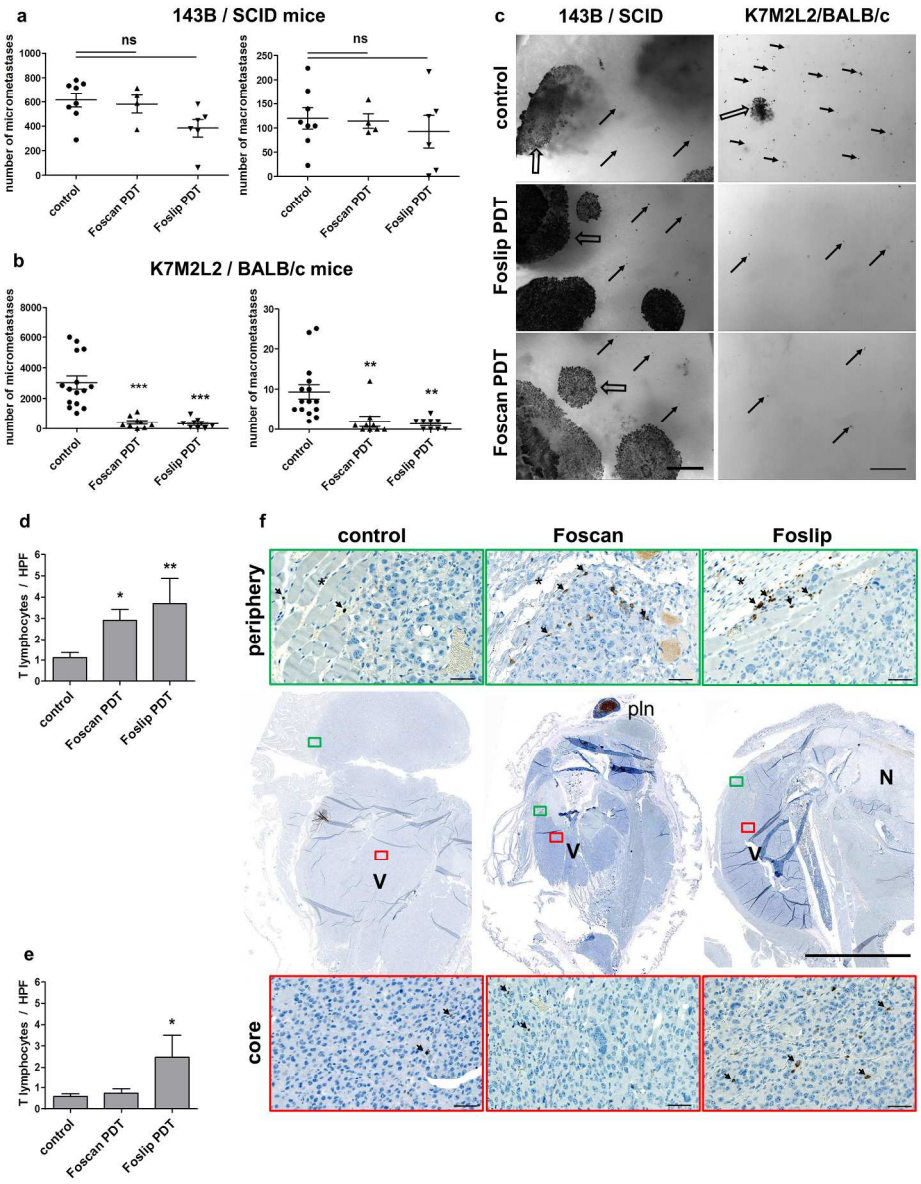

Figure 5. Effect of intratibial primary tumor treatment by PDT on pulmonary metastases and immune cell infiltration. (a) Ex vivo quantification of X-Gal stained 143B/LacZ cell-derived metastases on the surface of whole mounts of lungs collected from SCID mice at sacrifice 14 days after PDT. The data indicate the numbers of pulmonary micrometastases per lung (diameter < 0.1mm, left panel) and of pulmonary macrometastases (diameter > 0.1mm, right panel) in individual mice of the indicated treatment groups. The numbers of lungs analyzed in the different experimental groups are shown by the number of corresponding symbols in the figures. (b) Ex vivo quantification of X-Gal stained K7M2L2/LacZ cells on whole mounts of lungs collected from BALB/c mice at sacrifice 10 days after treatment. Data analysis as described in (a). (c) Representative images of X-gal–stained metastatic nodules on whole mounts of lungs of SCID mice and BALB/c mice. Black arrows point to pulmonary micrometastases and the open black arrow to a macrometastasis. Scale bar, 200 µm. (d) Mean (± SEM) number of T-lymphocytes per high power field (HPF) in primary tumor periphery. (e) Mean (± SEM) number of T-lymphocytes per high power field (HPF) in primary tumor core. (f) Representative images of H&E stained 5 µm sections of intratibial tumors collected

10 days after PDT from BALB/c mice treated as indicated. T-lymphocytes were identified by immunohistochemistry for the CD3 antigen (arrows) in the core (red rectangle) and at the periphery (green rectangle) of the tumors. V: viable tumor tissue, N: necrotic tumor tissue, pln: popliteal lymph node (on slide positive tissue control), *: soft tissue adjacent to the tumor. Scale bars: low magnification panel, 5 mm, high magnification panels, 50 µm. * $P < 0.05$, ** $P < 0.01$, *** $P < 0.001$, PDT-treated groups vs. control, n.s.: not significant.

259x329mm (300 x 300 DPI)

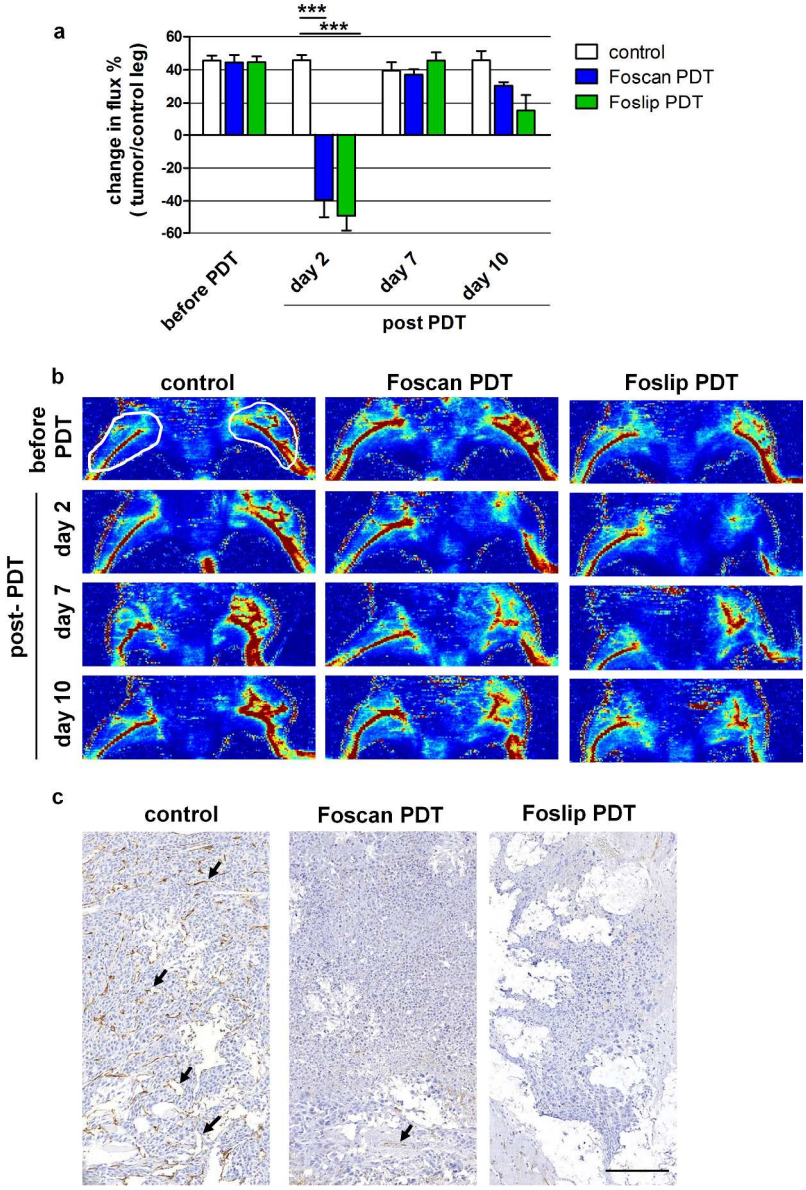

Figure 6. Effect of primary tumor treatment by Foscan or Foslip-based PDT on hind limb blood flow in the syngeneic K7M2L2/BALB/c osteosarcoma mouse model. (a) Blood flow in control and tumor-bearing hind limbs was measured with a laser Doppler perfusion imager in the regions of interest (ROI) (as indicated in b), and the data collected from 12 mice per treatment group on indicated experimental days are presented as percent change in perfusion (flux) of tumor compared to normal tissue, *** $P < 0.001$ PDT- treated vs. control. (b) Images of hind limb perfusion taken on indicated experimental days from representative mice of the different experimental groups. White circles indicate ROI for laser Doppler image analysis. (c) Representative images of CD31 immunostained 10 μm sections of intratibial tumors collected from representative mice of the indicated treatment groups on day 2 after PDT. Black arrows point to CD31-stained endothelial cells, scale bar 250 μm.

306x456mm (300 x 300 DPI)